ACS APPLIED MATERIALS & INTERFACES

Research Article

www.acsami.org

Stretchable Silver Nanowire–Elastomer Composite Microelectrodes with Tailored Electrical Properties

Vincent Martinez, Flurin Stauffer, Mohammed O. Adagunodo, Csaba Forro, Janos Vörös, and Alexandre Larmagnac*

Laboratory of Biosensors and Bioelectronics, Institute for Biomedical Engineering, ETH Zurich, Gloriastrasse 35, ETZ F76, CH-8092 Zurich, Switzerland

Supporting Information

ABSTRACT: We introduce a photolithography process compatible with soft and rigid substrates, enabling the fabrication of complex 3D interconnected patterns of silver nanowire (AgNW) networks embedded in polydimethylsiloxane (PDMS). Dimensions of the AgNW micropatterns are controlled within the film plane by photolithography, whereas thickness is controlled via a novel and uniform deposition technique using centrifugation. We report the first systematic characterization of the electromechanical properties of such microelectrodes with finest stretchable feature of 15 μm. We observe a geometry-dependent behavior of the gauge factor not only by changing the thickness of the microelectrodes, as it has been commonly reported so far, but also by varying their lateral dimensions. The presented nanocomposites exhibited sheet resistances down to 0.6 Ω/sq, gauge factors ranging from 0.01 to 100, and stretchability above 50% uniaxial strain. This versatile process allows for the production of highly sensitive strain sensors and robust high-density stretchable conductors on a wafer scale with direct implications in mass production of stretchable electronic devices.

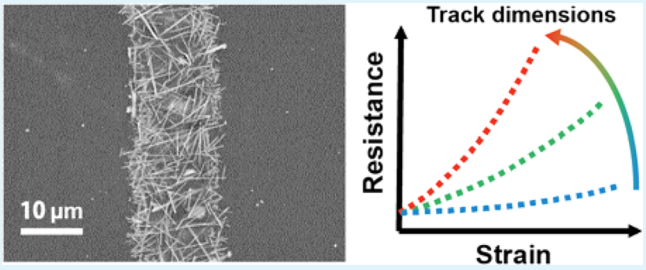

KEYWORDS: *stretchable conductors, silver nanowires, photolithography, strain sensors, vias, grid*

INTRODUCTION

Stretchable and transparent electrically conductive materials will enable the development of novel devices for everyday life, including flexible thin-film solar cells,[1] conformal electronics[2−4] like foldable displays,[5,6] and smart textiles[7,8] for personalized healthcare.[9,10] Recent research on stretchable conductors and strain sensors based on buckled nanoribbons,[11] microcracked gold thin films,[12] liquid metals,[13] graphene,[14,15] carbon nanotubes,[16−18] silver nanowires (AgNWs),[19−22] and different combinations of these[23−25] represent new alternatives to rigid conventional electronics. However, micropatterning of arbitrary stretchable electric circuits remains challenging for their future integration into microsensor arrays and bioelectronic applications.[26,27] AgNW–elastomer composite combines metallic conductivity and high aspect ratio conductive element structures prone to percolate at low filler distribution, enabling its use as highly stretchable conductors.[20] High conductivity allows for higher degree of miniaturization. Moreover, sensitive strain sensors can be produced by controlling the AgNW network dimensions in all three directions as demonstrated hereby.

So far, patterning nanowire networks was achieved by spraying[28] or drop casting a solution of AgNWs through a shadow mask[22] or dry transfer printing,[29] offering poor resolution. Higher resolution patterns down to 10 μm were achieved using either PDMS microfluidic channels and fit-to-flow method[30] or laser ablation of very thin AgNW films.[31] However, those processes do not allow high economical throughput. Recently, Lee et al. introduced a photolithography compatible process for the fabrication of planar miniature arbitrary patterns of AgNWs on substrates like glass or PDMS.[32] The limits of this process and the electrical performance of the obtained stretchable microelectrodes remain unclear. Herein, we report five major advances: (1) first fabrication of AgNW-based 3D stretchable microelectrodes for the realization of complex circuitry using photolithography, (2) novel uniform deposition of NW network based on centrifugation, (3) first electromechanical characterization of patterned AgNW microelectrodes, (4) observation of the geometry-dependent electromechanical behavior of AgNW tracks within the x–y plane (width and length) and thickness (z-plane) exhibiting tunable electrical properties such as sheet resistance and gauge factor, and (5) grid topology for high reproducibility of patterns below 20 μm.

RESULTS AND DISCUSSION

Wafer Scale Fabrication of 2D and 3D AgNW Microelectrodes on Various Substrates. Figure 1a illustrates the fabrication of arbitrary AgNW structures on rigid glass or silicon and on soft PDMS substrates for producing

Received: March 21, 2015
Accepted: May 27, 2015
Published: June 11, 2015

DOI: 10.1021/acsami.5b02508
ACS Appl. Mater. Interfaces 2015, 7, 13467−13475

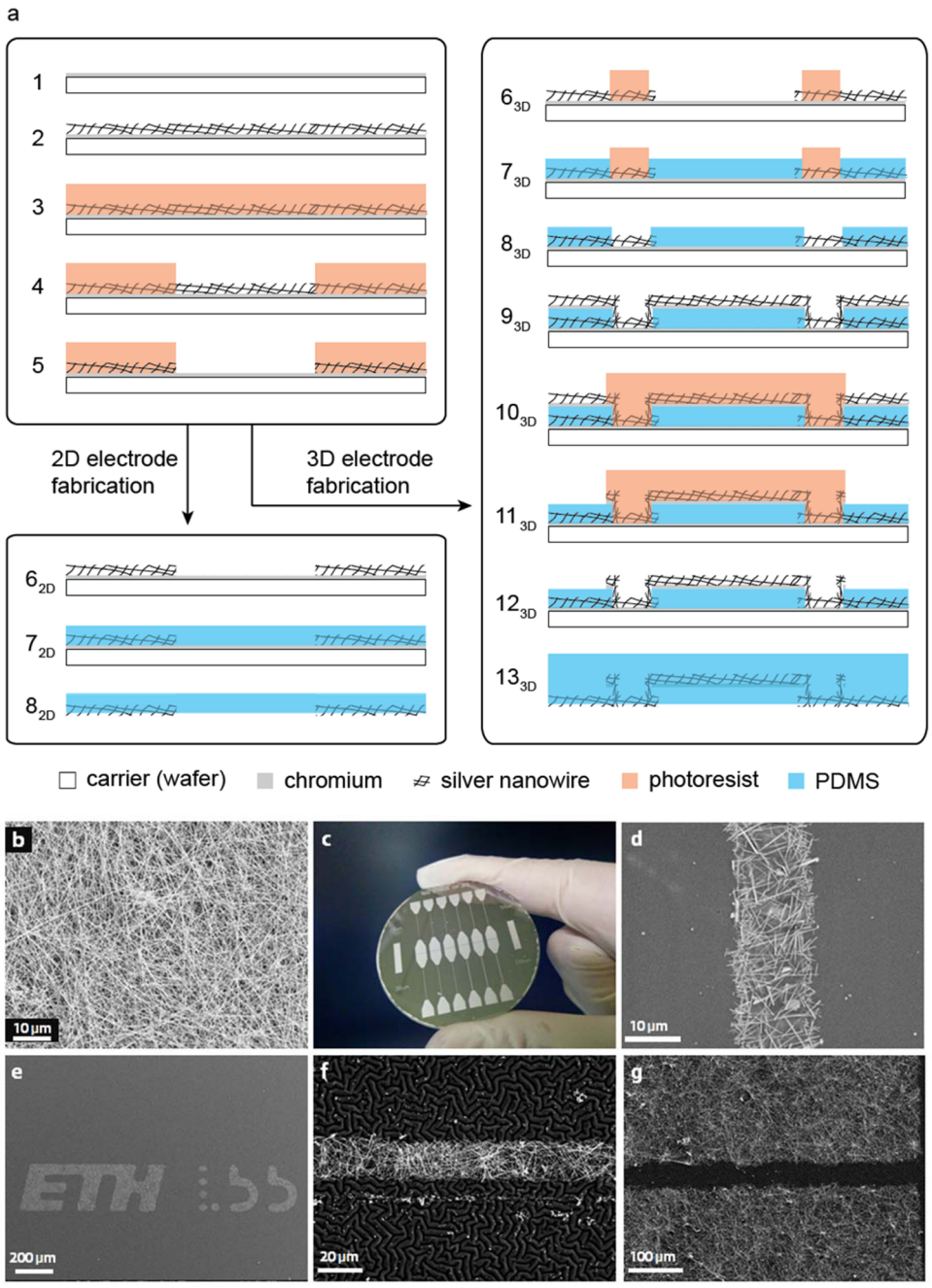

Figure 1. Microfabrication process for 2D and 3D microelectrodes with (a) schematic of the process flow: (1) chromium deposition, (2) AgNW deposition, (3) spin-coating of photoresist (PR), (4) PR exposure and development, and (5) AgNW etching followed by (6_{2D}) PR removal, (7_{2D}) PDMS spin-coating, (8_{2D}) peeling for 2D electrodes or (6_{3D}) second PR exposure and development, (7_{3D}) PDMS spin coating, (8_{3D}) PR removal, (9_{3D}) chromium and AgNW deposition, (10_{3D}) spin coating, exposure and development of PR, (11_{3D}) AgNW etching, (12_{3D}) PR removal, (13_{3D}) PDMS spin coating, and peeling for 3D electrodes. (b) SEM image of deposited AgNW film after centrifugation. (c) Optical image of wafer-scale production of AgNW microstructures, and SEM images of (d) patterned 12 μm wide AgNW line embedded in PDMS, (e) patterned ETH LBB logo embedded in PDMS, (f) patterned 20 μm wide AgNW line patterned on PDMS with wrinkled chromium layer, and (g) patterned 40 μm wide spacing between AgNWs on PDMS.

2D and 3D AgNW microelectrodes. Prior to any processing, a chromium layer is deposited on the glass substrate to prevent Si−O−Si bonds with PDMS and facilitate peeling (Figure 1a-1). A film of AgNWs is deposited on the substrate by centrifuging a solution of AgNWs dispersed in 2-propanol (Figure 1a-2). After drying (Figure 1b), micropatterns of AgNWs are produced on a wafer-scale (Figure 1c) using positive photolithography and wet etching (Figure 1a-3 to 5, see Experimental Section). For 2D microelectrodes, a layer of PDMS is then cast and spin-coated on top of the structures (Figure 1a-6_{2D} to 8_{2D}). After curing and peeling, the AgNWs are embedded just below the surface of the PDMS as previously reported (Figure 1d,e).[21] On glass surface (Figure 1a-3 to 6), resolution less than 10 μm could not be reproducibly obtained. This might be attributed to the higher development time that was necessary to expose the photoresist under the thick, nonfully transparent wire network. This overdevelopment and the strong scattering induced by the nanowires might have

DOI: 10.1021/acsami.5b02508
ACS Appl. Mater. Interfaces 2015, 7, 13467−13475

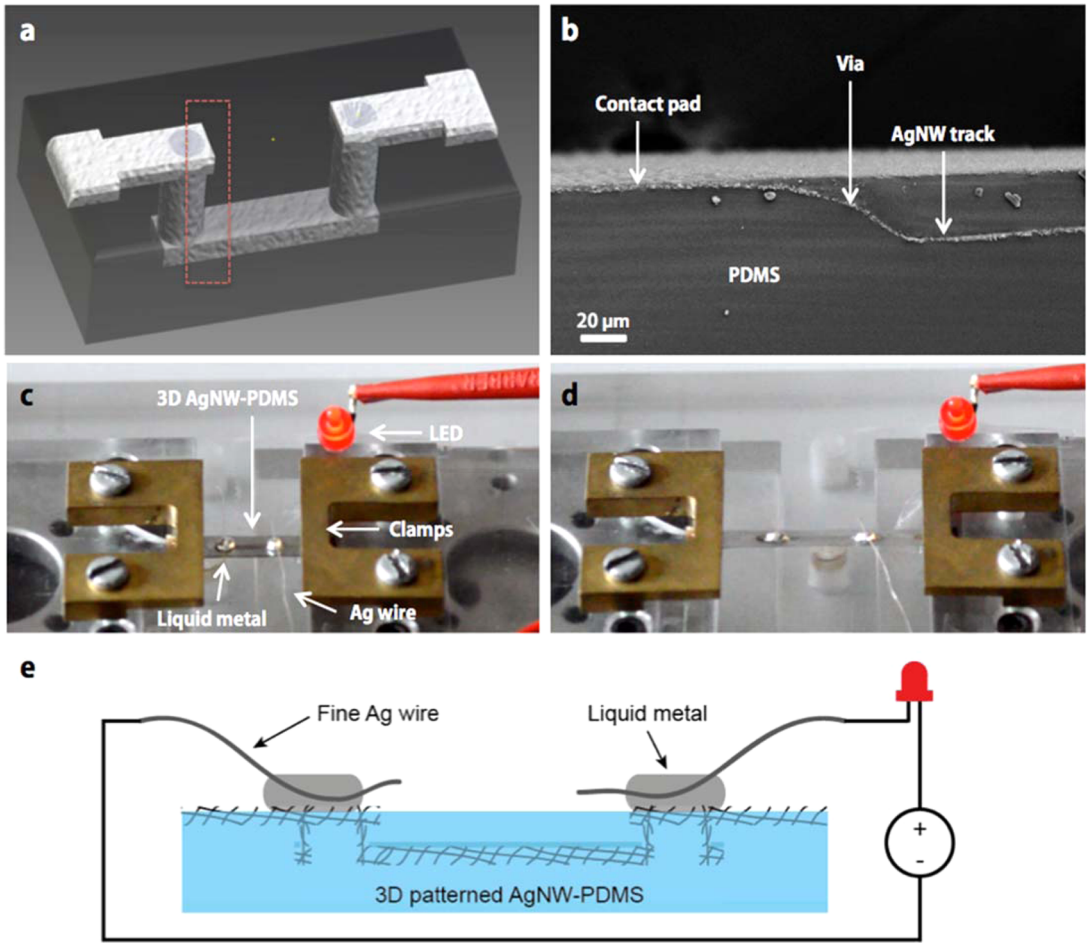

Figure 2. Feasibility of the 3D AgNW microelectrodes produced via the 3D fabrication process with (a) 3D schematics and (b) SEM picture of a via (indicated by the red box in (a)) with the corresponding sample mounted on a manual stretcher and connected in series with an LED using fine silver wires and liquid metal (c) at 0% strain showing a resistance of 136 Ω, (d) uniaxially stretched to 100% strain showing a resistance of 247 Ω, and (e) schematic illustration of the electrical connections.

enhanced inhomogeneous UV absorbance of the resist/AgNWs composite. The resulting inhomogeneous undercut photoresist tracks could lead to interrupted wire lines after silver etching for widths below 10 μm. For 3D microelectrodes, a thicker photoresist layer is used for patterning both the bottom AgNW electrode layer and for creating via structures in the PDMS using two successive exposure and development steps of the photoresist (Figure 1a-6_{3D}). After PDMS spin-coating, curing, and photoresist removal (Figure 1a-7_{3D}, 8_{3D}), a second chromium layer is evaporated onto the PDMS. A AgNW film is deposited (Figure 1a-9_{3D}) and patterned as on glass except that the resist is cured at room temperature for a week to avoid crack formation of the PDMS substrate due to thermal expansion (Figure 1a-10_{3D} to 13_{3D}, see Experimental Section). A shorter curing time would significantly improve the practicability of the process and will be investigated in future work. Photopatterning on silicone-based polymers such as PDMS usually requires oxygen plasma treatment[33] or metallization of the surface[12] to improve wettability and adhesion of the photoresist. Without the second chromium layer, the photoresist could not be properly processed, and only large structures of AgNWs were patterned. On PDMS surface, we achieved a resolution of 20 μm for tracks and 40 μm for spacings, as shown in parts f and g of Figure 1, respectively. After patterning, a layer of PDMS is spin coated over the AgNWs and cured to form the stretchable composite.

Feasibility of 3D Patterned Microelectrodes. One of the primary challenges in stretchable electronics is the fabrication of multilayer interconnects to increase the integration density. Recently, the fabrication of stretchable double-sided printed circuit boards with interconnecting vias was achieved by stencil printing a conductive composite elastomer on a PDMS substrate.[34] Guo et al. addressed this issue for photolithographically patterned gold tracks on PDMS,[35] but no equivalent technique for composite AgNW–PDMS was reported. We addressed this limitation by successively patterning on glass and on PDMS to produce 3D dual-layer structures interconnected by vias of 1 mm in diameter (see Figure 2a). During drop-casting deposition of the second AgNW layer, the NWs coat the inner walls of the vias, thus electrically interconnecting the top and bottom layers. Figure 2b is an SEM image of the cross-section of a via showing the physical interconnection between both layers. The slope profile of the via is induced by collapsing of the PDMS, which covered the side walls of the photoresist pillars after photoresist removal (see Supporting Information Figure S1). The functionality of stretchable vias similar to that represented in Figure 2 was recorded (see Supporting Information movie). The resistance of a 500 μm wide track interconnecting two

DOI: 10.1021/acsami.5b02508
ACS Appl. Mater. Interfaces 2015, 7, 13467−13475

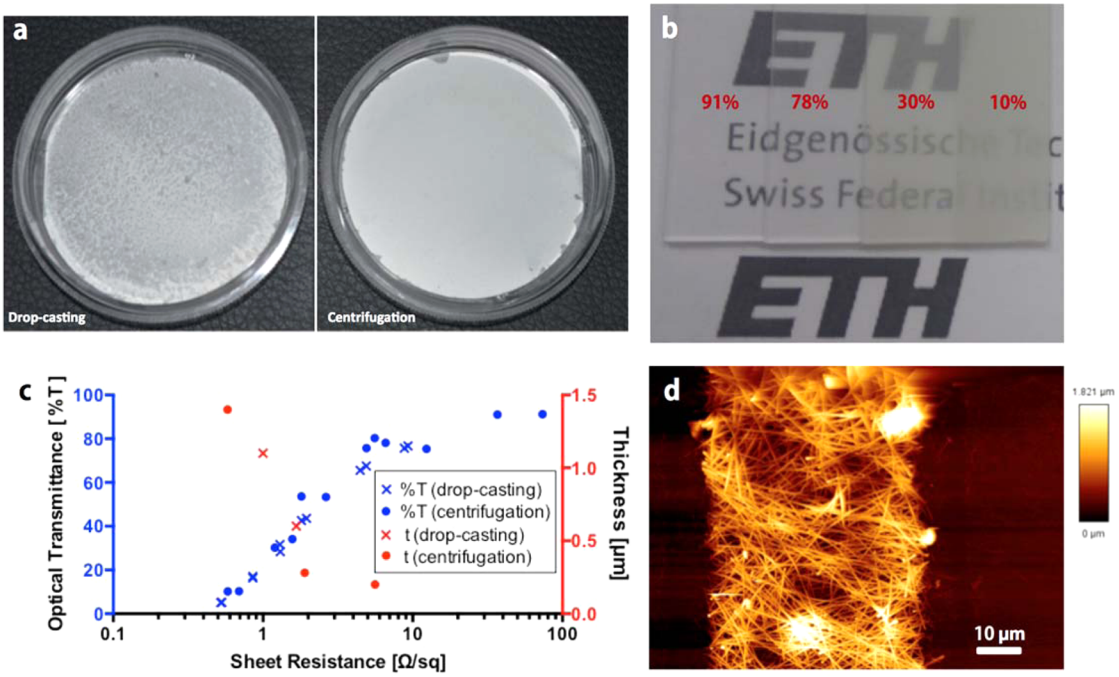

Figure 3. Characterization of the transmittance, electrical resistance, and topography of the AgNW films with (a) large-scale deposition images on 2 in. wafers using drop-casting and centrifugation showing a better homogeneity for the centrifugation technique, (b) glass slides coated with different transmittance of AgNW networks deposited by centrifugation, (c) optical transmittance and thickness as a function of sheet resistance for AgNW films deposited on glass after drop-casting and centrifugation, and (d) AFM scan of a AgNW track with a sheet resistance of 1.7 Ω/sq and 23%T for an average network thickness of 590 nm.

pads increased by less than a factor of 2 when stretched up to 100%, demonstrating the feasibility of the technique (Figure 2c,d). Figure 2e shows a schematic diagram of the electrical setup using liquid metal to provide a stable electrical contact to the electrodes under stretch without influencing the sample. This unique combined approach enables the fabrication of robust dual-layer interconnects for high-density AgNW-based 3D stretchable electrodes.

Homogeneous and Controlled AgNW Deposition on Various Substrates. The deposition of a homogeneous AgNW film of controlled thickness is required to obtain AgNW micropatterns with arbitrary dimensions in a reproducible manner. Although the resistance of large samples can be tuned by changing the amount of deposited nanowires,[22] homogeneous and controlled deposition is difficult to achieve using drop casting because of the "coffee ring effect".[36] Spray coating can achieve better homogeneity but requires high back pressure and small droplet size optimization.[37] Rod coating is used for large scale deposition of thin AgNW films, however, it remains unclear if thick and homogeneous films can be produced.[38] Spin-coating is suited only for thin nanowire networks (or requires repeated deposition steps) and is not economical due to loss of material.[39] Radial forces and fast evaporation rate may also lead to a nonuniform coating network. Vacuum filtration is usually the preferred method because the AgNWs are deposited homogeneously at a density proportional to the volume of the filtered solution. Although such films can be easily transferred onto sticky substrates like PDMS, transferring onto glass or silicon wafers is challenging.[29]

To address all of these issues, we introduce a new and simple technique based on centrifugation (see Supporting Information Figure S2) that allows depositing thick, homogeneous nanowire films without waste of material using standard lab equipment. The advantage of centrifugation compared to drop-casting is that a stable nanowire network is formed before evaporation of the solvent, preventing the coffee ring effect (Figure 3a). The film thickness and transparency are directly determined by the nanowire concentration and solution volume (Figure 3b). Because of the strong centrifugal forces, only horizontal surfaces are coated with nanowires, leaving vertical walls uncoated. The optical and electrical properties of such AgNW films were similar to films obtained after drop-casting (Figure 3c), and the morphology of nanowires did not differ from one technique to the other (see Supporting Information Figure S3). The sheet resistance of AgNW films exhibits a bulk-like behavior below 80−90% transmittance and a percolation behavior at higher transparencies following an exponential increase of the sheet resistance, as reported elsewhere.[40]

The film thickness was measured using atomic force microscopy (AFM). Figure 3d shows an AFM scan of a well-defined NW track with average thicknesses of 590 nm for a sheet resistance measured of 1.7 Ω/sq. There is no principle limit to the thickness of the film, as it can be increased by using a higher concentration of AgNWs solution or repeating deposition steps without waste of material.

AgNW Microelectrodes with Tunable Electromechanical Properties. We investigated the electromechanical properties of 2D AgNW−PDMS composite microelectrodes with high aspect ratio (length of 1 cm, width of 20−100 μm) by using progressive strain cycling. We particularly comment on the limit for stretchable single line patterns with less than 20 μm features. After PDMS casting, curing, and peeling, we observed a consistent increase in sheet resistance of AgNW films by a factor of 2 for films with a low transmittance of 13%, corresponding to other reported results,[21] and a factor of 10 for films with a transmittance of 51% (Figures 3c and 4a). For

DOI: 10.1021/acsami.5b02508
ACS Appl. Mater. Interfaces 2015, 7, 13467−13475

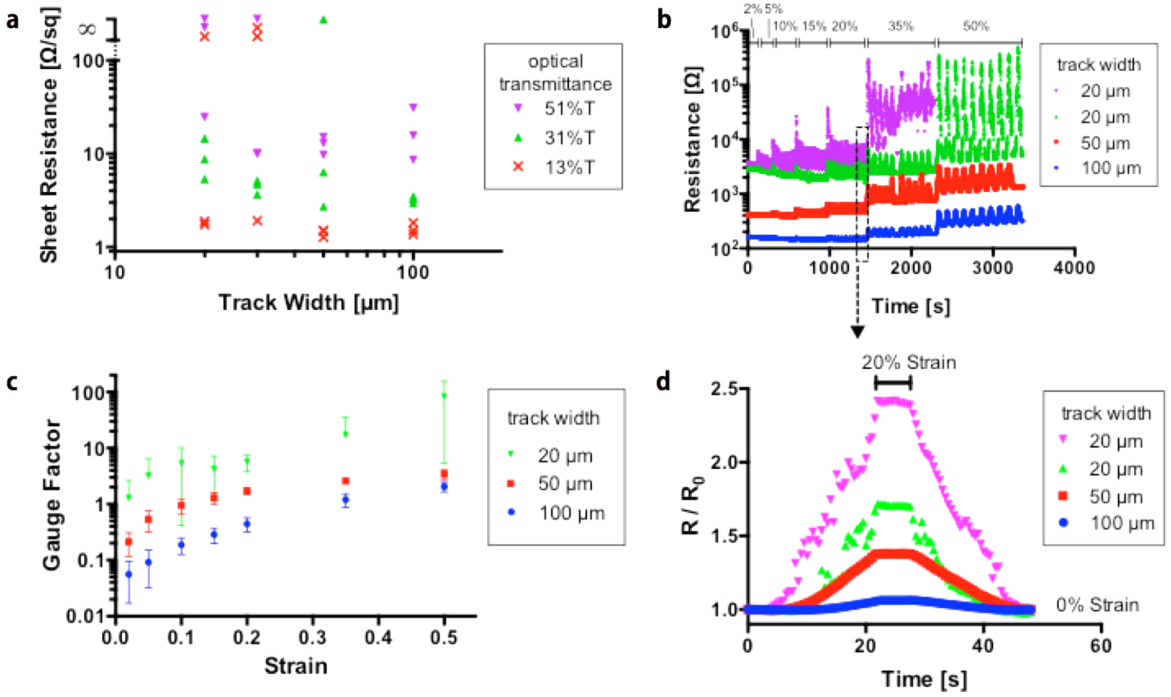

Figure 4. Electromechanical characterization of 1 cm long, patterned AgNW tracks embedded in PDMS with (a) sheet resistance after peeling off the sample as a function of the track width for different AgNW concentrations corresponding to optical transmittances of 13%T, 31%T and 51%T, (b) evolution of the resistance during progressive strain cycling with five cycles without waiting time and five more cycles with 5 s waiting time per strain level at maximal strain (2%, 5%, 10%, 20%, 35% 50%) of samples with 6%T and different track widths, (c) gauge factor as a function of strain for different track widths (6%T) measured with progressive strain cycling (3 samples each), (d) the 10th stretch cycle with 20% strain for different track widths (6%T). The data from two different samples with a track width of 20 μm prepared identically are displayed in (b) and (d) to show the different electrical responses due to defects or local inhomogeneities in the AgNW film. Samples with track widths of 50 μm or wider did not show this discrepancy.

samples with transmittance >60%, the sheet resistance dramatically increased and could not be reliably measured. This might be explained by the mechanical stress exerted on the NWs while peeling off the sample from the supporting substrate. Indeed, when increasing the adhesion between the substrate and the PDMS, i.e., by removing the chromium layer, and consequently increasing the force necessary to peel the samples, we observed an even more significant increase in sheet resistance (data not shown). Using a sacrificial layer between the glass substrate and the PDMS layer may further reduce this effect. Decreasing the width of the patterns from 100 μm down to 20 μm tended to increase the sheet resistance and the proportion of nonconductive tracks (data points with infinite resistance) as shown in Figure 4a, which is in agreement with the percolation theory. Track widths well below the length of single AgNWs (20−50 μm) are more likely to result in interrupted (no percolation) or poorly stretchable lines due to (i) local inhomogeneities in the AgNW film resulting in bottleneck regions prone to early electrical failure and (ii) the decreased aspect ratio of the etched AgNWs. Although smaller patterns were achieved (1 mm long, 10 μm wide), no electrical conductivity could be reproducibly measured, indicating the limit of our photolithography process for randomly deposited AgNWs.

Similar microelectrodes patterned out of a thicker and less transparent film (6%T) were stretched for 10 cycles at progressively increasing strains. While low strains (<20%) induced fully reversible change in resistance, a permanent loss of conductive pathways was observed after the first loading−unloading cycle for strains >20% (Figure 4b), as reported elsewhere.[21,22] The resistance of 50 and 100 μm wide tracks (R_0 < 500 Ω) increases by less than a factor of 2 and 3.3 after applying 35% and 50% strain cycles, respectively. In this composite, one observes two buckling phenomena. First, nanowire films embedded in the surface layer lead to surface buckling after strain release as demonstrated by Xu et al,[21] Second, buckling of single nanowires that are fully embedded in the elastomer matrix as reported in a similar composite.[41] Dark field images reveal the formation of broken nanowires while stretching above 50% and buckled nanowires after relaxation (see Supporting Information Figure S4). During the stretching phase, the PDMS channels containing the nanowires expand in the direction of the strain, which increases radial compression forces and thus friction forces at the AgNW−PDMS interface. The resulting stretching forces applied to the nanowires may exceed their ultimate tensile strength and break them when the samples are stretched at very high strains >50%. During relaxation phase, the elastic PDMS channels are moving in the opposite direction by applying a compressive force to the nanowires, which induces the observed buckling (see Supporting Information Figure S4). Buckling of nanowires not sliding back to their initial position in the matrix increases the loss of nanowire contacts after stretching consequently increasing the resistance of the track. The change in resistance became more reversible and linear after five cycles, meaning that the destructive process mainly occurs when samples are stretched to an unprecedented applied strain. Narrow tracks with a width of 20 μm showed inconsistent behavior with a markedly different electrical response to strain (see Figure 4b where data from two identically prepared samples with a track

DOI: 10.1021/acsami.5b02508
ACS Appl. Mater. Interfaces 2015, 7, 13467−13475

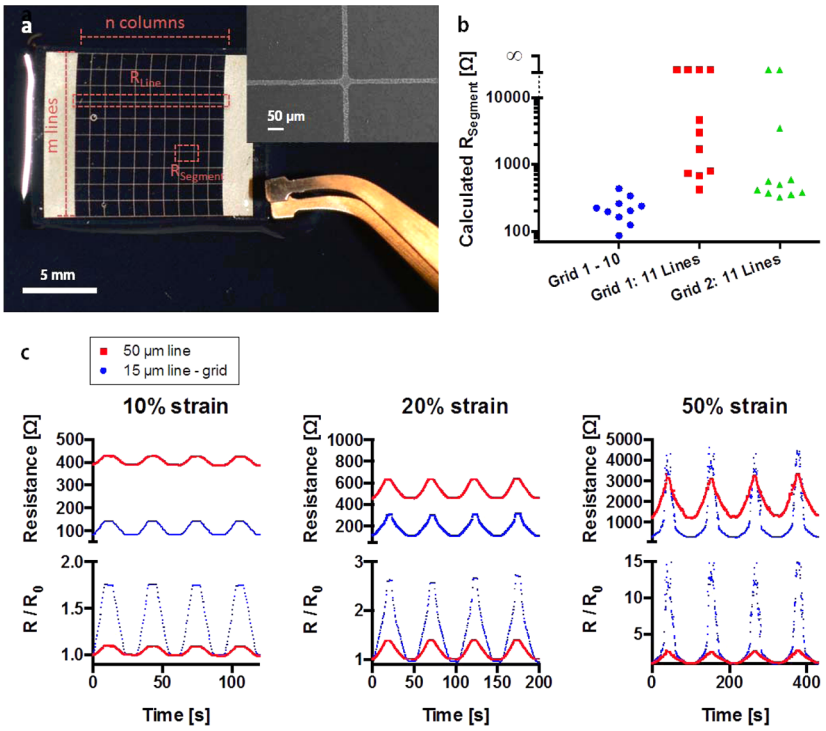

Figure 5. Characterization of AgNW–PDMS grids with 15 μm line width and 1 mm pitch, averaged optical transmittance of 96%, and mean resistance of 266 Ω (n = 10) with (a) optical image of a grid (inset: SEM image of a grid node), (b) calculated values of $R_{segment}$ derived from the measured grid resistances R_{grid} (with $R_{segment} = m/n \times R_{grid}$) compared to the values of $R_{segment}$ derived from the measured resistances of single lines R_{line} cut out of two grids (with $R_{segment} = R_{line}/n$), and (c) relative change in resistance of a grid compared to that of a 50 μm wide and 1 cm long single line upon strain cycling (four cycles with 5 s breaks at 0% and at maximum cycling strain).

width of 20 μm are shown), although their initial resistances were similar while wider tracks performed more consistently, as shown in Figure 4c. Percolating conductive filler networks are inherently subject to hysteresis attributable to two main components: intrinsic time-dependent viscoelastic properties of the elastomeric matrix and adhesion properties of the conductive fillers to the matrix.[22] Both influence the rearrangement of the nanowires inside the matrix, consequently affecting the electrical behavior of the sensor or conductor. We show in the Supporting Information Figure S5 the hysteresis behavior over one stretching cycle for different geometries and the long-term drift with fatigue strain cycling as depicted in Supporting Information Figure S6.

The gauge factor (GF) or the sensitivity to strain is defined as $(\Delta R/R_0)/\varepsilon$, where R_0 is the initial electrical resistance and ΔR is the change in resistance for a given applied strain ε. So far, highly sensitive strain or pressure sensors based on composite elastomers such as carbon black/polymer composite,[42] carbon nanotube/polymer composite[18] or silver nanoparticles/polymer composite[43] were mostly designed by changing the thickness of the pattern or the filler content. Recent work on AgNW–PDMS showed (i) resistive strain sensors exhibiting a tunable gauge factor from 2 to 14 by controlling the amount of deposited AgNWs[22] and (ii) capacitive strain sensors with a gauge factor up to 1.[21] Low density AgNW networks change from homogeneous to inhomogeneous under strain with emerging bottleneck locations that significantly increase the resistance of the percolative cluster. Thanks to the photolithography process, we can even further decrease the number of percolative pathways by narrowing down the tracks, thus increasing the GF, significantly enabling, to the best of our knowledge, the most sensitive strain sensors based on AgNWs with gauge factor of 100 for 20 μm wide electrodes (6%T) at strains of 50%, as depicted in Figure 4c. Whereas the GF of a single AgNW is ~2 as reported elsewhere,[44] GFs from 0.01 up to 100 were obtained by changing the dimensions of the patterned AgNW–PDMS composite (see Figure 4c,d), suggesting that robust stretchable electronic circuits as well as highly sensitive strain sensors can be produced simultaneously on the same wafer by simply etching away the required amount of AgNWs. Figure 4d shows the electrical response of such tracks with different widths for the same applied strain cycle. The yield of our fabrication process was observed to decrease from nearly 100% for track width above 50 μm down to approximately 50% for track width below 20 μm for the reasons mentioned previously.

A Grid Topology for a 100% Yield. We introduced a grid topology to overcome this limitation. The resistance R_{grid} of an ideal grid structure as shown in Figure 5a, where the resistance of each segment is $R_{segment}$ is calculated according to Kirchhoff's law $R_{grid} = n/m \times R_{segment}$, with m the number of interconnected parallel lines and n the number of segments in series. Samples with such topology (m = 11, n = 10, track width of 15 μm, and pitch of 1 mm) exhibited high optical transmittance of 96% (Figure 5a), with sheet resistances of 92 Ω/sq comparable with ITO (typical transmittance of 80% for 10 Ω/sq),[45] CNT/metal NW mesh (transmittance of 92% for ~100 Ω/sq),[46] or e-beam lithographically patterned Ag grids (transmittance of 91% for 6.5 Ω/sq)[47] with the significant advantage of being stretchable. Because of the higher probability to find conductive pathways in the grid topology, the yield for a batch of 10 samples was 100%. Two of these grids were sliced into 11 individual lines that appeared to be more resistive than expected, some even

DOI: 10.1021/acsami.5b02508
ACS Appl. Mater. Interfaces 2015, 7, 13467–13475

being interrupted. This is summarized in Figure 5b, where the calculated values of $R_{segment}$ derived from the measured resistances of 10 grids are compared to the values from the isolated 11 lines of two grids. Such grids have a low electrical resistance and a low hysteresis while exhibiting gauge factors similar to that of narrow tracks, which are challenging to reproduce with a high yield and may be interesting for strain sensing applications (see Figure 5c and Supporting Information Figures S5 and S7). This topology enables the fabrication of stretchable electronics with tunable optical and electrical properties such as sheet resistance and gauge factor in a unique and independent manner. Until now, strain sensors with high initial resistance were most appropriate for high gauge factor with low strain applications. By decoupling the sheet resistance with the gauge factor using our grid approach, we undoubtedly offer more flexibility to the design of strain sensors.

CONCLUSION

In this work, we presented a deposition technique based on centrifugation and a photolithography process for the patterning of microsized AgNW structures on rigid or elastomeric substrates. We demonstrated that this process can be applied to fabricate complex 3D multilayer structures of AgNWs embedded in PDMS on a wafer-scale with tunable optical and electrical properties and may extend the use of AgNW−PDMS composites in stretchable electronics and strain sensing applications.

EXPERIMENTAL SECTION

Nanowires Deposition. Immediately after treating the surface of glass or PDMS substrates with air plasma (Harrick Plasma PDC-32G, air pressure of 0.02 mbar, RF power of 18 W, 30 s), the AgNWs were deposited by centrifugation (centrifuge 5810 R, Eppendorf) of a solution of AgNWs (diameter of 115 nm, length of 20−50 μm, 0.5 vol % in IPA, Sigma-Aldrich) at 4000 rpm (G-force ≈ 2500) for 1 min. The substrates were placed in sealed custom-made containers placed in the machine (see Supporting Information Figure S2). Drop-casting used as comparative deposition method was done by allowing the AgNWs to sediment for 2 h on similarly prepared substrates in a closed chamber to prevent solvent evaporation. In both methods, the supernatant or solvent lying above the deposited AgNW film was removed with a pipet and the film was sintered on a hot plate at 150 °C for 20 min. The deposited nanowire density, and therefore, the transmittance, was controlled by changing the concentration and volume of the nanowire solution.

Characterization. We measured the regular optical transmittance of the AgNW networks using a fiber coupled UV/NIR enhanced PDA array spectrometer (Cypher X, B&W Tek) coupled with a tungsten halogen light source (BPS120, B&W Tek) after nanowires deposition on glass or glass/chromium. Uncoated substrates were used to subtract the reference spectra. Transmittance spectra were observed at three different spots (with an area of ∼10 mm^2) per sample. To characterize the samples, we used the optical transmittance at a wavelength of 550 nm. Scanning electron microscopic (SEM) images were taken using a Zeiss SUPRA 50 VP with an accelerating voltage between 5 and 10 kV. Optical dark-field pictures were obtained using an electron multiplying charge-coupled device (EM-CCD, Hamamatsu C9100-13) with a Zeiss Axiovert 200.

Photolithography Process. Referred to in the text as Figure 1a-3 to 5: Prior to the AgNWs deposition, the glass substrate was coated with a 15 nm thick chromium layer. After AgNWs deposition, an 11 μm thick layer of positive photoresist ma-P 1275 HV (Micro Resist Technology GmbH, Germany) was spin-coated at 1000 rpm followed by a 30 min resting interval. Softbake was performed with a slow ramping including stops at 60, 90, and 120 °C for 2 min. The samples were cooled down to room temperature with a minimal resting interval of 1 h. Next, the samples were exposed with a Karl Süss MJB3 UV400 mask aligner for an exposure dose of 7 mJ/cm^2 at λ = 405 nm and a total of 160 s (multiple exposure, four cycles, 1 min waiting time). The exposed photoresist was developed within 5 min in the inorganic alkaline developer Ma-D 331 (Micro Resist Technology GmbH, Germany) with a rinsing step in DI water. To etch the AgNWs, we immersed the sample for 15 s in a gold etchant solution (Sigma-Aldrich, Gold etchant nickel compatible). Removal of the unexposed photoresist and cleaning of the samples were done by successive immersion of the samples in the remover mr-Rem 400 (Micro Resist Technology GmbH, Germany), acetone, 2-propanol and DI water for 5 min each. Then, samples were dried on a hot plate at 100 °C for 10 min. PDMS (Sylgard 184) was mixed with a standard ratio of 10:1 (Thinky Mixer ARE-250) and spin-coated at 500 rpm for 30 s, cured at 60 °C overnight, and peeled in ethanol.

Referred to in the text as Figure 1a-10$_{3D}$ to 13$_{3D}$: For creating 3D electrodes, AgNWs were patterned on glass as described previously using a thick layer of 40 μm of positive photoresist ma-P 1275 HV. The thick layer of photoresist was soft baked only up to 110 °C (instead of 120 °C) to avoid bubble formation. After exposure, development and AgNW etching to obtain the first pattern, the remaining photoresist was UV exposed and developed a second time for creating pillars to protect the location of the vias before spin-coating a 20 μm thin PDMS layer (5000 rpm, 60 s). After curing overnight at 60 °C, the thin layer of PDMS covering the pillars was removed mechanically and the resist was stripped in acetone, thus leaving openings for vias. After evaporating a 15 nm thick chromium layer on the perforated PDMS substrate, a second AgNW layer was deposited by drop-casting and patterned as on glass except that the resist was cured at room temperature for a week to avoid crack formation. Finally, a second layer of PDMS was spin-coated and cured overnight at 60 °C.

Electrical and Mechanical Setup. The stretching of the samples was conducted using a tensile testing machine (DO-FB0.5TS, Zwick/Roell) with a constant strain rate of 1.0%/s. The original length of stretched part was 22 mm. The resistance was measured every 0.5 s with a digital multimeter (Agilent 34401A) using 2-terminal sensing with eutectic gallium−indium (Sigma-Aldrich) and either with copper clamps or fine silver wires for contacting the sample. Progressive cycling experiments were done with 10 strain cycles per strain level. The progressively increased strain levels were 2%, 5%, 10%, 15%, 20%, 35%, and 50%. The gauge factor was calculated using cycle 10 (with waiting time of 5 s at maximal strain) for each strain level.

AFM Measurements. The AFM images were taken with a NanoWizard I BioAFM from JPK Instruments using a NSC15 cantilever from Mikromasch (spring constant of 40 N/m) with a line rate of 0.1 Hz in intermittent contact mode (Amplitude Modulation). Thickness was calculated by averaging the topography on AFM scan areas (100 × 100 μm^2).

ASSOCIATED CONTENT

Supporting Information

Functionality of stretchable vias (AVI). Additional experimental details with materials, methods and figures (PDF). The Supporting Information is available free of charge on the ACS Publications website at DOI: 10.1021/acsami.5b02508.

AUTHOR INFORMATION

Corresponding Author

*E-mail: larmagnac@biomed.ee.ethz.ch.

Author Contributions

The manuscript was written through contributions of all authors. All authors have given approval to the final version of the manuscript. V.M. and F.S. contributed equally.

Notes

The authors declare no competing financial interest.

DOI: 10.1021/acsami.5b02508
ACS Appl. Mater. Interfaces 2015, 7, 13467−13475

■ ACKNOWLEDGMENTS

We thank F. Mettler and T. Kinkeldei for technical help with the tensile test machine and S. Wheeler and M. Lanz for their valuable technical support. We acknowledge the assistance and support of the Center for Microscopy and Image Analysis, University of Zurich, for performing scanning electron microscopy experiments. We thank the EU FP7 NEUWalk, the Swiss Nanotera SpineRepair projects, and ETH Zurich for funding.

■ REFERENCES

(1) Schubert, M. B.; Werner, J. H. Flexible Solar Cells for Clothing. *Mater. Today* **2006**, *9* (6), 42−50.
(2) Kim, D. H.; Lu, N. S.; Huang, Y. G.; Rogers, J. A. Materials for Stretchable Electronics in Bioinspired and Biointegrated Devices. *MRS Bull.* **2012**, *37* (3), 226−235.
(3) Wagner, S.; Bauer, S. Materials for Stretchable Electronics. *MRS Bull.* **2012**, *37* (3), 207−217.
(4) Kaltenbrunner, M.; Sekitani, T.; Reeder, J.; Yokota, T.; Kuribara, K.; Tokuhara, T.; Drack, M.; Schwodiauer, R.; Graz, I.; Bauer-Gogonea, S.; Bauer, S.; Someya, T. An Ultra-Lightweight Design for Imperceptible Plastic Electronics. *Nature* **2013**, *499* (7459), 458−463.
(5) White, M. S.; Kaltenbrunner, M.; Glowacki, E. D.; Gutnichenko, K.; Kettlgruber, G.; Graz, I.; Aazou, S.; Ulbricht, C.; Egbe, D. A. M.; Miron, M. C.; Major, Z.; Scharber, M. C.; Sekitani, T.; Someya, T.; Bauer, S.; Sariciftci, N. S. Ultrathin, Highly Flexible and Stretchable PLEDs. *Nature Photonics* **2013**, *7* (10), 811−816.
(6) Sekitani, T.; Nakajima, H.; Maeda, H.; Fukushima, T.; Aida, T.; Hata, K.; Someya, T. Stretchable Active-Matrix Organic Light-Emitting Diode Display Using Printable Elastic Conductors. *Nature Mater.* **2009**, *8* (6), 494−499.
(7) Cherenack, K.; van Pieterson, L. Smart textiles: Challenges and Opportunities. *J. Appl. Phys.* **2012**, *112* (9), 091301.
(8) Cochrane, C.; Koncar, V.; Lewandowski, M.; Dufour, C. Design and Development of a Flexible Strain Sensor for Textile Structures Based on a Conductive Polymer Composite. *Sensors* **2007**, *7* (4), 473−492.
(9) Webb, R. C.; Bonifas, A. P.; Behnaz, A.; Zhang, Y. H.; Yu, K. J.; Cheng, H. Y.; Shi, M. X.; Bian, Z. G.; Liu, Z. J.; Kim, Y. S.; Yeo, W. H.; Park, J. S.; Song, J. Z.; Li, Y. H.; Huang, Y. G.; Gorbach, A. M.; Rogers, J. A. Ultrathin Conformal Devices for Precise and Continuous Thermal Characterization of Human Skin. *Nature Mater.* **2013**, *12* (10), 938−944.
(10) Pantelopoulos, A.; Bourbakis, N. G. A Survey on Wearable Sensor-Based Systems for Health Monitoring and Prognosis. *IEEE Trans. Syst. Man Cybern., Part C: Appl. Rev.* **2010**, *40* (1), 1−12.
(11) Sun, Y.; Choi, W. M.; Jiang, H.; Huang, Y. Y.; Rogers, J. A. Controlled Buckling of Semiconductor Nanoribbons for Stretchable Electronics. *Nature Nano* **2006**, *1* (3), 201−207.
(12) Adrega, T.; Lacour, S. P. Stretchable Gold Conductors Embedded in PDMS and Patterned by Photolithography: Fabrication and Electromechanical Characterization. *J. Micromech. Microeng.* **2010**, *20* (5), 055025−055033.
(13) Park, J.; Wang, S.; Li, M.; Ahn, C.; Hyun, J. K.; Kim, D. S.; Kim, D. K.; Rogers, J. A.; Huang, Y.; Jeon, S. Three-Dimensional Nanonetworks for Giant Stretchability in Dielectrics and Conductors. *Nature Commun.* **2012**, *3*, 916.
(14) Kim, K. S.; Zhao, Y.; Jang, H.; Lee, S. Y.; Kim, J. M.; Kim, K. S.; Ahn, J. H.; Kim, P.; Choi, J. Y.; Hong, B. H. Large-Scale Pattern Growth of Graphene Films for Stretchable Transparent Electrodes. *Nature* **2009**, *457* (7230), 706−710.
(15) Chen, Z. P.; Ren, W. C.; Gao, L. B.; Liu, B. L.; Pei, S. F.; Cheng, H. M. Three-Dimensional Flexible and Conductive Interconnected Graphene Networks Grown by Chemical Vapour Deposition. *Nature Mater.* **2011**, *10* (6), 424−428.
(16) Lipomi, D. J.; Vosgueritchian, M.; Tee, B. C. K.; Hellstrom, S. L.; Lee, J. A.; Fox, C. H.; Bao, Z. N. Skin-like Pressure and Strain Sensors Based on Transparent Elastic Films of Carbon Nanotubes. *Nature Nanotechnol.* **2011**, *6* (12), 788−792.
(17) Xiao, L.; Chen, Z.; Feng, C.; Liu, L.; Bai, Z. Q.; Wang, Y.; Qian, L.; Zhang, Y. Y.; Li, Q. Q.; Jiang, K. L.; Fan, S. S. Flexible, Stretchable, Transparent Carbon Nanotube Thin Film Loudspeakers. *Nano Lett.* **2008**, *8* (12), 4539−4545.
(18) Yamada, T.; Hayamizu, Y.; Yamamoto, Y.; Yomogida, Y.; Izadi-Najafabadi, A.; Futaba, D. N.; Hata, K. A Stretchable Carbon Nanotube Strain Sensor for Human-Motion Detection. *Nature Nanotechnol.* **2011**, *6* (5), 296−301.
(19) Hu, W. L.; Niu, X. F.; Zhao, R.; Pei, Q. B. Elastomeric Transparent Capacitive Sensors Based on an Interpenetrating Composite of Silver Nanowires and Polyurethane. *Appl. Phys. Lett.* **2013**, *102* (8), 083303.
(20) Lee, P.; Lee, J.; Lee, H.; Yeo, J.; Hong, S.; Nam, K. H.; Lee, D.; Lee, S. S.; Ko, S. H. Highly Stretchable and Highly Conductive Metal Electrode by Very Long Metal Nanowire Percolation Network. *Adv. Mater.* **2012**, *24* (25), 3326−3332.
(21) Xu, F.; Zhu, Y. Highly Conductive and Stretchable Silver Nanowire Conductors. *Adv. Mater.* **2012**, *24* (37), 5117−5122.
(22) Amjadi, M.; Pichitpajongkit, A.; Lee, S.; Ryu, S.; Park, I. Highly Stretchable and Sensitive Strain Sensor Based on Silver Nanowire−Elastomer Nanocomposite. *ACS Nano* **2014**, *8* (5), 5154−5163.
(23) Lee, M. S.; Lee, K.; Kim, S. Y.; Lee, H.; Park, J.; Choi, K. H.; Kim, H. K.; Kim, D. G.; Lee, D. Y.; Nam, S.; Park, J. U. High-Performance, Transparent, and Stretchable Electrodes Using Graphene−Metal Nanowire Hybrid Structures. *Nano Lett.* **2013**, *13* (6), 2814−2821.
(24) Woo, J. Y.; Kim, K. K.; Lee, J.; Kim, J. T.; Han, C. S. Highly Conductive and Stretchable Ag Nanowire/Carbon Nanotube Hybrid Conductors. *Nanotechnology* **2014**, *25* (28), 285203.
(25) Xu, Z.; Liu, Z.; Sun, H. Y.; Gao, C. Highly Electrically Conductive Ag-Doped Graphene Fibers as Stretchable Conductors. *Adv. Mater.* **2013**, *25* (23), 3249−3253.
(26) Park, M.; Park, J.; Jeong, U. Design of Conductive Composite Elastomers for Stretchable Electronics. *Nano Today* **2014**, *9* (2), 244−260.
(27) Park, J.; You, I.; Shin, S.; Jeong, U. Material Approaches to Stretchable Strain Sensors. *ChemPhysChem* **2015**, *16* (6), 1155−1163.
(28) Liang, J. J.; Li, L.; Niu, X. F.; Yu, Z. B.; Pei, Q. B. Elastomeric Polymer Light-Emitting Devices and Displays. *Nature Photonics* **2013**, *7* (10), 817−824.
(29) Madaria, A. R.; Kumar, A.; Ishikawa, F. N.; Zhou, C. W. Uniform, Highly Conductive, and Patterned Transparent Films of a Percolating Silver Nanowire Network on Rigid and Flexible Substrates Using a Dry Transfer Technique. *Nano Res.* **2010**, *3* (8), 564−573.
(30) Tao, Y.; Tao, Y. X.; Wang, L. Y.; Wang, B. B.; Yang, Z. G.; Tai, Y. L. High-Reproducibility, Flexible Conductive Patterns Fabricated with Silver Nanowire by Drop or Fit-to-Flow Method. *Nanoscale Res. Lett.* **2013**, *8* (147), 1−5.
(31) Hong, S.; Yeo, J.; Lee, J.; Lee, H.; Lee, P.; Lee, S. S.; Ko, S. H. Selective Laser Direct Patterning of Silver Nanowire Percolation Network Transparent Conductor for Capacitive Touch Panel. *J. Nanosci. Nanotechnol.* **2015**, *15* (3), 2317−2323.
(32) Ahn, Y.; Lee, H.; Lee, D.; Lee, Y. Highly Conductive and Flexible Silver Nanowire-Based Microelectrodes on Biocompatible Hydrogel. *ACS Appl. Mater. Interfaces* **2014**, *6* (21), 18401−18407.
(33) Chen, W. Q.; Lam, R. H. W.; Fu, J. P. Photolithographic Surface Micromachining of Polydimethylsiloxane (PDMS). *Lab Chip* **2012**, *12* (2), 391−395.
(34) Larmagnac, A.; Eggenberger, S.; Janossy, H.; Voros, J. Stretchable Electronics Based on Ag-PDMS composites. *Sci. Rep.* **2014**, *4*, 7254.
(35) Guo, L.; DeWeerth, S. P. An Effective Lift-Off Method for Patterning High-Density Gold Interconnects on an Elastomeric Substrate. *Small* **2010**, *6* (24), 2847−2852.
(36) Langley, D.; Giusti, G.; Mayousse, C.; Celle, C.; Bellet, D.; Simonato, J. P. Flexible Transparent Conductive Materials Based on

DOI: 10.1021/acsami.5b02508
ACS Appl. Mater. Interfaces 2015, 7, 13467−13475

Silver Nanowire Networks: a Review. *Nanotechnology* **2013**, *24* (45), 452001.
(37) Scardaci, V.; Coull, R.; Lyons, P. E.; Rickard, D.; Coleman, J. N. Spray Deposition of Highly Transparent, Low-Resistance Networks of Silver Nanowires over Large Areas. *Small* **2011**, *7* (18), 2621−2628.
(38) Hu, L.; Kim, H. S.; Lee, J.-Y.; Peumans, P.; Cui, Y. Scalable Coating and Properties of Transparent, Flexible, Silver Nanowire Electrodes. *ACS Nano* **2010**, *4* (5), 2955−2963.
(39) Leem, D.-S.; Edwards, A.; Faist, M.; Nelson, J.; Bradley, D. D. C.; de Mello, J. C. Efficient Organic Solar Cells with Solution-Processed Silver Nanowire Electrodes. *Adv. Mater.* **2011**, *23* (38), 4371−4375.
(40) De, S.; King, P. J.; Lyons, P. E.; Khan, U.; Coleman, J. N. Size Effects and the Problem with Percolation in Nanostructured Transparent Conductors. *ACS Nano* **2010**, *4* (12), 7064−7072.
(41) Weili, H.; Xiaofan, N.; Lu, L.; Sungryul, Y.; Zhibin, Y.; Qibing, P. Intrinsically Stretchable Transparent Electrodes Based on Silver-Nanowire−Crosslinked-Polyacrylate Composites. *Nanotechnology* **2012**, *23* (34), 344002.
(42) Mattmann, C.; Clemens, F.; Troster, G. Sensor for Measuring Strain in Textile. *Sensors* **2008**, *8* (6), 3719−3732.
(43) Park, M.; Im, J.; Shin, M.; Min, Y.; Park, J.; Cho, H.; Park, S.; Shim, M. B.; Jeon, S.; Chung, D. Y.; Bae, J.; Park, J.; Jeong, U.; Kim, K. Highly Stretchable Electric Circuits from a Composite Material of Silver Nanoparticles and Elastomeric Fibres. *Nature Nanotechnol.* **2012**, *7* (12), 803−809.
(44) McCarthy, E. K.; Bellew, A. T.; Sader, J. E.; Boland, J. J. Poisson's Ratio of Individual Metal Nanowires. *Nature Commun.* **2014**, *5*, 4336.
(45) Kulkarni, A. K.; Schulz, K. H.; Lim, T. S.; Khan, M. Dependence of the Sheet Resistance of Indium-Tin-Oxide Thin Films on Grain Size and Grain Orientation Determined from X-ray Diffraction Techniques. *Thin Solid Films* **1999**, *345* (2), 273−277.
(46) Lee, J. Y.; Connor, S. T.; Cui, Y.; Peumans, P. Solution-Processed Metal Nanowire Mesh Transparent Electrodes. *Nano Lett.* **2008**, *8* (2), 689−692.
(47) van de Groep, J. V.; Spinelli, P.; Polman, A. Transparent Conducting Silver Nanowire Networks. *Nano Lett.* **2012**, *12* (6), 3138−3144.

DOI: 10.1021/acsami.5b02508
ACS Appl. Mater. Interfaces 2015, 7, 13467−13475